

Industrial and Engineering Paper

Cite this article: El-Sawy S, Nawaz W, Osama M, Tekin A (2020). Low-cost thin-film passive RFID circuits and detector system. *International Journal of Microwave and Wireless Technologies* **12**, 356–366. <https://doi.org/10.1017/S175907871900151X>

Received: 20 December 2018
Revised: 6 November 2019
Accepted: 16 November 2019
First published online: 6 January 2020

Key words:

Low cost; mutual inductance; passive RFID; planar finger capacitance; planar spiral inductance; reader circuit; wireless charger

Author for correspondence:

Salma El-Sawy,
E-mail: salma.elsawy@ozu.edu.tr

Low-cost thin-film passive RFID circuits and detector system

Salma El-Sawy , Wasim Nawaz , Mohamed Osama and Ahmet Tekin

Özyeğin University, OZU-X Building, Istanbul, Turkey

Abstract

This paper discusses the design of chip-less RFID tags of a standard pocket size of 69 mm by 156 mm. These tags are based on lumped elements of copper metal traces constructed on a thin polyamide flexible substrate. Moreover, a low-cost single-chip Bluetooth detector circuit system is demonstrated. Two different detection methods: variable coil load coupling and optical light intensity detection were combined to yield 256 unique ID codes. In the first method, by utilizing simple 4 MHz digital drivers and an integrated analog to digital converter (ADC) in the reader controller; various inductively coupled resonant loads corresponding to multiple distinct tags could be differentiated, yielding eight different (3-bit) ID codes. The additional via-based hole pattern reflectometer method creates additional 32 distinct levels (5-bit) utilizing 650 nm visible light-emitting diode and a simple trans-impedance operational along with the same analog ADC pins of a Bluetooth controller. The printed circuit board trace coil on the two-layer low-cost FR-4 waterproof sealed detector unit is simultaneously used as a Qi wireless power receiver to charge the 120 mAh 2450 Lithium Polymer (LiR) battery. The device could remain operational for more than a month with a single charge; remaining connected with a mobile device and enabling 10 readouts daily.

Introduction

RFIDs have been steadily taking part in many aspects of our lives in various applications. In the past few decades, researchers have shown a noticeable interest in RFID systems. Many systems were presented with their different techniques and aspects. A brief classification for RFID tags in the market in terms of power, communication range and protocol, and data processing is elaborated in Fig. 1 [1]. RFID tags introduced to the market were categorized according to a different point of views: power, communication range, programmability, and data processing. From the power point of view, the RFID systems are sub-categorized into active [2], semi-active [3, 4], and passive [5–7]. Moreover, from the communication range point of view, they are sub-categorized into three main categories: close coupled [7, 8], remote coupled, and long range [9, 10]. Nowadays, several applications facilitate the use of simple passive RFID tags to limit the cost of the ID tag unit and introduce relatively more complexity to the reader design. Several RFID tag technologies managed to give several appealing inexpensive solutions and sustain the functionality of the given system, such as low-cost, thin, light weighted, and flexible tags. Those mentioned tags show good mechanical and electrical properties. RFID tags being flexible is an advantageous point as they can be stored easily and are preferable for daily use. In order to ensure the sustainability of the flexible substrate for the desired RFID applications, the fabricated tags should be subjected to several movements such as bending, folding, and twisting repeatedly to test their robustness. According to [11–13], the flexible tags showed reversible electrical characteristics during the bending tests. Many passive RFID tags use transmission lines and micro-strip patch antennas, most of which are used for long-range and high-frequency applications [9, 10]. On the other hand, applications with lower frequencies in the order of 10 MHz are used more for relatively very short-range applications. Hence, ID tag design depends very much on lumped element planar patterns such as spiral inductance and interdigitated capacitances [8]. Most current RFID systems involve a silicon chip that would set a limit on the total achievable system cost. However, there are some applications that may have an extra degree of freedom with a reader complexity which leads to a relatively low-cost for the ID tag unit. Several researchers showed a great interest in RFID systems. In [14], a low-profile chip-less RFID tag for wrist band applications is presented; however, it requires tuning of slot parameters during its application to get desired resonant frequency. Moreover, a low-cost chip-less RFID tag based on split-ring resonators is demonstrated in [15], but it cannot be used in applications that require flexible tags. The paper proposes a system with negligible ID tag unit cost, and also a cost-effective reader. The design of the proposed RFID tag depends mainly on some passive resonant distinct load circuits and via patterns that are traced on a planar flexible printed circuit board (PCB). The PCB is light-weight 0.1 mm thin polyamide substrate along with the

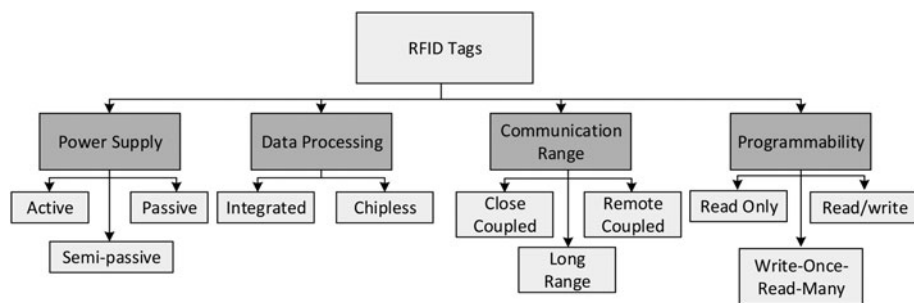


Fig. 1. The classification of RFID tags in the market.

18 μm copper clad for the lumped device traces. With the planar spiral inductance and the interdigitated finger capacitance combination on the tag side, distinguishable signal-level variations were obtained at the detector. On the detector side, in addition to the previously mentioned RF signature verification, an extra module is embedded, which employs an additional optical front-end to detect the reflected light pattern and intensity corresponding to via pattern around black silkscreened focus area. This combination of distinct optical and RF patterns along with the corresponding encryption results in a fully functional system that is low-cost, portable, and suitable for daily use. The paper presents in detail the planar passive resonance device tags and the wireless charging opto-electronic detector sub-system designs with the corresponding measurement results. The rest of this paper is organized as follows: the section “RFID design” elaborates on the RFID tag design, where the design of passive structures will be discussed. The section “Lumped elements calculations” presents the calculation methods for the planar capacitance and inductance. The section “Simulations and measurements versus calculations” shows the simulation results used to verify the previously mentioned calculations and compares them with the measurements. The section “Tag circuits and systems” presents the circuit details of the proposed peak voltage detector and wireless charger combo system, and optical front-end of the detector. The system simulations and measurements are provided in the section “Measurements”. Finally, the section “Conclusion” concludes the main findings of this study.

RFID design

As the challenging part of the idea, the proposed RFID tags are chip-less and use very simple planar circuit elements: inductance and capacitance utilizing only copper traces of 18 μm thickness on a flexible substrate. The design is implemented on a single-layer thin flexible PCB (Kapton), which has a low relative dielectric of 3.4 compared to the normal FR-4 dielectric of 4.7. This section introduces the design of two prototype RFID tags with a target size of 69 mm \times 159 mm suitable for containing the largest lumped element geometries desired. The first tag has a circular spiral inductance that is equivalent to 556 nH. The coil is formed of three turns with a copper trace width of 0.2 mm, a gap of 0.2 mm as well, and an external diameter of total 25.7 mm, as shown in Fig. 2(a). The second tag has a larger rectangular spiral inductance of 26 μH along with an interdigitated finger capacitance providing an equivalent capacitance of 296 pF. The rectangular spiral inductance is designed with two different trace thicknesses of 0.2 and 0.8 mm to have the best area to inductance ratio, a gap of 0.2 mm, an outer width of 37.7 mm, and an outer length of 62.6 mm. The 45-degree tilted edges ensure robustness for the coil toward any

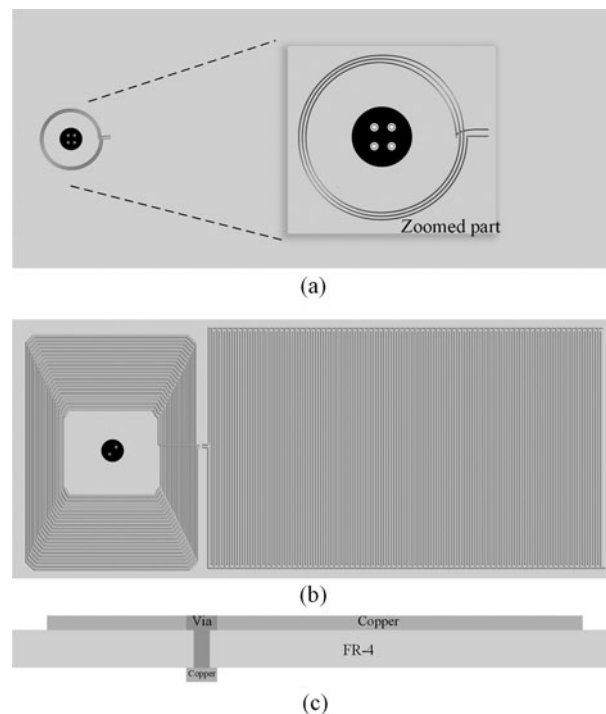


Fig. 2. The design of the two proposed RFID tags: (a) Tag A: the first tag with circular spiral inductance. (b) Tag B: the second tag with the chamfered rectangular inductance and interdigitated finger capacitance. (c) Cross-section of tag B defining the layers.

damage as 90-degree transition may suffer from breakdown or failure during active use. The interdigitated finger capacitance is composed of 182 fingers. Each finger is of 65.5 mm length, with a copper trace width of 0.4 mm and a gap of 0.2 mm, which are designed to get a large capacitance to area ratio. This particular tag design is shown in Fig. 2(b). In the middle of tag A, a pattern of four holes is added for the light reflection detection. As for tag B, a pattern of two holes is inserted for the validation of the two detection methods on these limited number of prototypes.

Lumped elements calculations

Since designing reliably distinguishable RFID tags with only lumped element traces has been the main target of this study, it is necessary to have a reliable approximate value for the first cut lumped elements necessary for the tag design. Many would consider that the advanced 3D EM simulation tools were a good choice for extracting these values, but they might consume a significant amount of simulation time, processing power, and

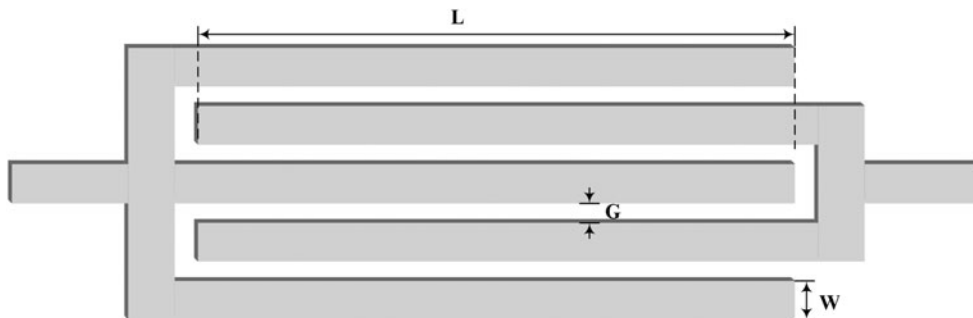


Fig. 3. Five fingers interdigitated finger capacitance.

may easily result in inaccurate results when the geometries of interest come to be sophisticated and large [16]. In order to speed up the design of the RFID tags, this section elaborates on fast calculation techniques for interdigitated finger capacitance and the various geometries of a spiral inductance to obtain a close estimate of resonances on the target tag structures.

Capacitance calculations

In order to go through calculations, there is a need to define the interdigitated finger capacitance's geometry and related parameters. Figure 3 illustrates an interdigitated finger capacitance of $n=5$ where n is the number of fingers, G is the gap between two fingers, L is the common length between two fingers, and W is the width of a single finger capacitance. The calculation method to be mentioned is only valid for capacitance with a finger thickness relatively small compared to its width. The capacitance value is dependent on the gap to metal ratio, which is defined as the metallization ratio represented by equation (1):

$$\eta = \frac{W}{W + G}. \quad (1)$$

This type of capacitance is excited by the differential voltage. The top comb with positive voltage V_+ and the bottom comb with negative voltage V_- . Consequently, the middle distance between two successive fingers would be virtually grounded and the capacitance will be defined as given in Fig. 4(a), where the capacitance is divided into two categories, interior capacitance noted as C_I and exterior capacitance noted as C_E . This structures' equivalent model is illustrated in Fig. 4(b). From Fig. 4(b), the overall capacitance value C_T can be obtained in terms of the internal and external capacitance, C_I and C_E respectively, as shown in equation (2):

$$C_T = (N - 3) \times \frac{C_I}{2} + \frac{2(C_I \times C_E)}{C_I + C_E}, \quad N > 3. \quad (2)$$

According to [17, 18], C_I and C_E are defined by equations (3) and (4) respectively, and the complete elliptic integral of $K(k)$, $K(k')$ is necessary, where k and k' are the modulus and the complementary modulus, respectively:

$$C_I = \varepsilon_0(\varepsilon_s + 1)L \frac{K(k_{I\infty})}{K(k'_{I\infty})}, \quad (3)$$

$$C_E = \varepsilon_0(\varepsilon_s + 1)L \frac{K(k_{E\infty})}{K(k'_{E\infty})}, \quad (4)$$

where ε_0 is the absolute dielectric constant of air, and ε_s is the relative dielectric of the substrate. The modulus and complementary modulus of the internal capacitance differ from one case to another according to the height of the dielectric and how many dielectric materials the design has. As for this work, only the substrate is available and the upper dielectric is an infinite layer of air [17]. Hence the values of k and K' will be defined for this case by equations (5) and (6):

$$k_{E\infty} = \frac{2\sqrt{\eta}}{1 + \eta}, \quad k'_{E\infty} = \sqrt{1 - k_{E\infty}^2}, \quad (5)$$

$$k_{I\infty} = \sin\left(\frac{\pi}{2}\eta\right), \quad k'_{I\infty} = \sqrt{1 - k_{I\infty}^2}. \quad (6)$$

As mentioned, it is necessary to solve the complete elliptic integral of the first kind which is defined by equation (7):

$$K(k) = \int_0^1 \frac{dt}{(1 - t^2)(1 - (kt)^2)}. \quad (7)$$

Due to the complexity of solving this integral, a MATLAB code was developed to ease the evaluation of the integral and obtaining the value of total capacitance.

Inductance calculations

The initial tag prototypes in this work have considered two extreme geometries for spiral inductances. One of them is a regular circular spiral inductance with a limited number of turns as shown in Fig. 5(a), and the other one is a rectangular shape with dense turn ratio as shown in Fig. 5(b). Two different wire thicknesses were utilized along the vertical and horizontal tracks, utilizing the given area for maximum inductance value. As regards to the circular coil, its inductance can be simply calculated according to [19]; depending on the current sheet approximation, its inductance is defined by equation (10), where μ is the permeability, n is the number of turns, d_{avg} is the average distance between the outer and inner diameter, ρ is the fill factor, and C_I are the coefficients dependent on the geometry as given in Table 1. This method takes into consideration the symmetry of the spiral geometry and hence offers an approximation for the sides of the spirals by symmetrical current sheets of equivalent

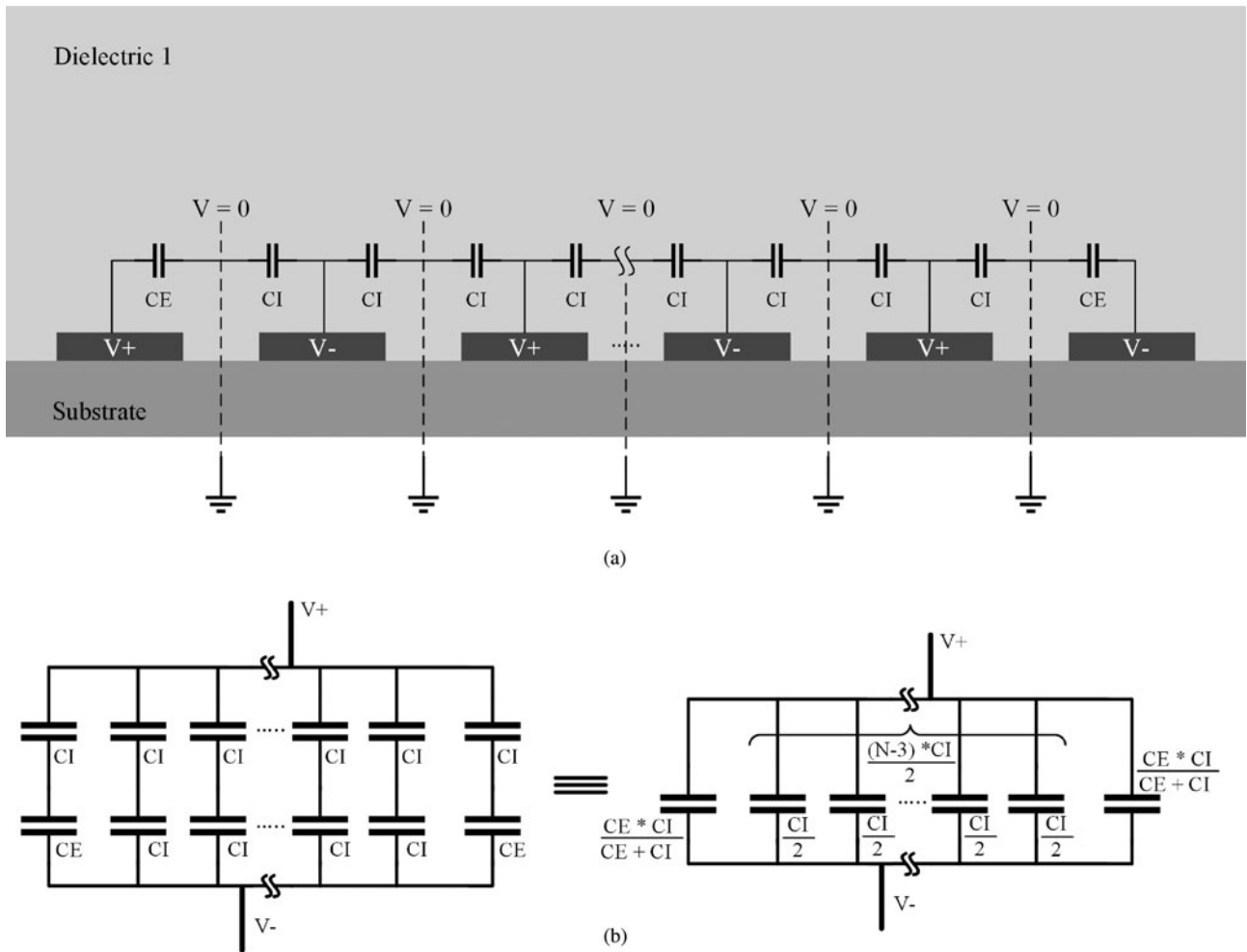


Fig. 4. Capacitance model: (a) Capacitance between fingers on substrate. (b) Equivalent circuit model.

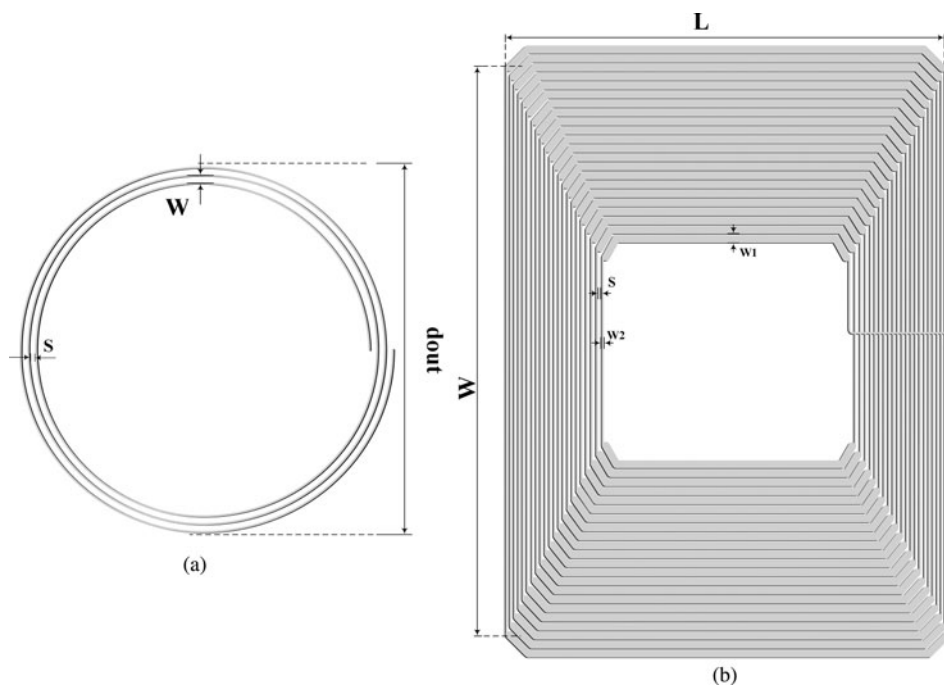


Fig. 5. Spiral inductance: (a) Circular spiral inductance. (b) Rectangular spiral inductance.

Table 1. Coefficients for current sheet expression

Geometry	c_1	c_2	c_3	c_4
Circular	1.00	2.46	0.00	0.20
Square based	1.27	2.07	0.18	0.13
Rectangular based	1.27	2.07	0.18	0.13

current densities. Moreover, as elaborated in [19], the total inductance of a square structure is the sum of four identical values obtained by the current sheets, since the four sides are identical.

$$d_{\text{avg}} = \frac{d_{\text{out}} + d_{\text{in}}}{2}, \quad (8)$$

$$\rho = \frac{d_{\text{out}} - d_{\text{in}}}{d_{\text{out}} + d_{\text{in}}}, \quad (9)$$

$$L_{\text{circ}} = \frac{\mu n^2 d_{\text{avg}} c_1}{2} \left(\ln\left(\frac{c_2}{\rho}\right) + c_3 \rho + c_4 \rho^2 \right). \quad (10)$$

Therefore, using this information, an assumption can be made that one side of the given rectangular coil inductance can be represented by equation (11), with two identical values for the length of the rectangular coil and two others for the width. Given all the equations needed to get the total inductance of this unique coil.

$$L_{\text{side}} = \frac{\mu n^2 d_{\text{avg,side}} c_1}{8} \left(\ln\left(\frac{c_2}{\rho}\right) + c_3 \rho + c_4 \rho^2 \right), \quad (11)$$

$$L_{\text{rect, total}} = 2 (L_{\text{side=W}} + L_{\text{side=L}}). \quad (12)$$

Simulations and measurements versus calculations

In order to prove that the driven calculation methods are sufficient, simulations and measurements are needed to verify the equations' veracity.

Capacitance simulations and measurements versus calculations

As stated in [16], the simulation tools cannot get a reliable value of capacitance when the number of fingers exceeds 50. Consequently, it is compulsory to verify the calculations and simulations for a smaller number of fingers. Using ANSYS Maxwell software, the equivalent capacitance value was acquired for several capacitances of a different number of fingers and compared with calculations for a capacitance of a finger length 65.5 mm, a gap of 0.2 mm, and a finger width of 0.4 mm. Figure 6 plots the comparison of both simulated and calculated values of capacitance for a number of fingers ranging from 4 to 32. Since this simple calculation method more or less converges with the simulation results, it is more appropriate to build a test prototype with a capacitance value of 183 fingers, and compare the results with the measured values after fabrication, as shown in Table 2. The error between the calculated and measured value was around 1%.

Inductance simulations and measurements

Verifying the inductance value was a relatively easier task compared to the capacitance. Table 3 elaborates the results of the calculated, simulated, and measured values of both proposed circular and rectangular spiral inductances. Inductor simulations were as well conducted with the help of ANSYS Maxwell CAD EM design tool to extract estimate values for those specific geometries. The circular spiral inductance had an outer diameter of 25.7 mm, a wire thickness of 0.2 mm, a gap of 0.2 mm, and three number of turns, while the rectangular spiral inductance was designed

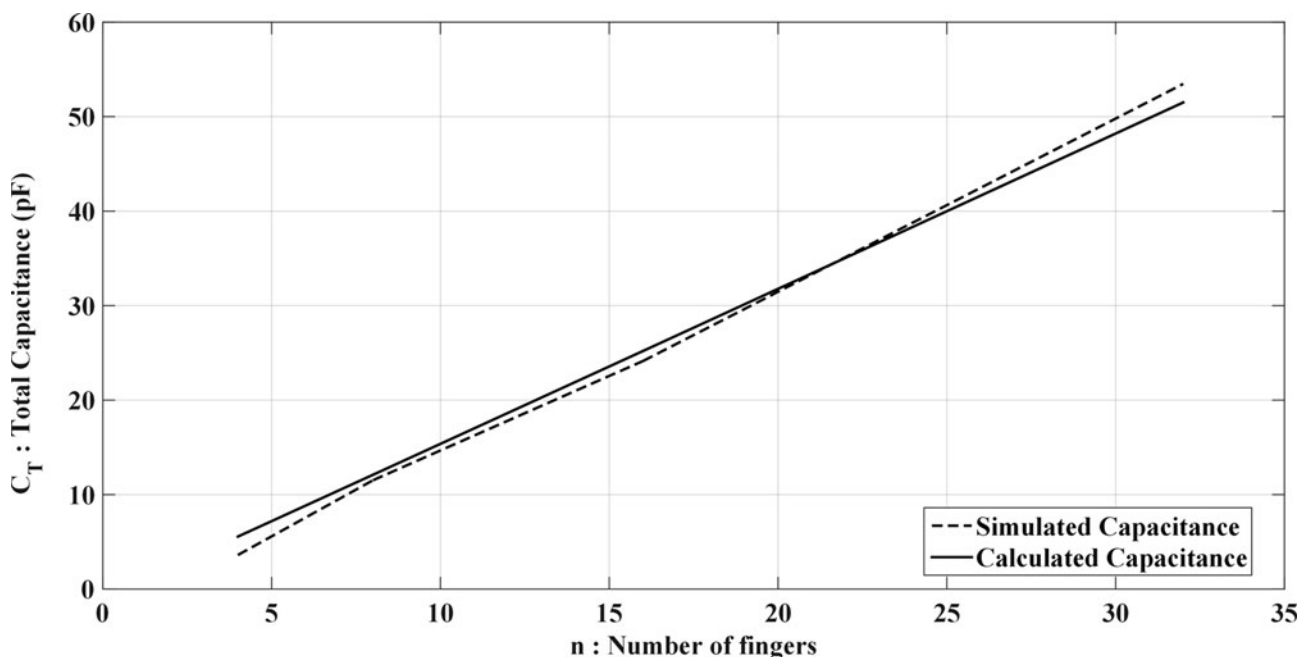
**Fig. 6.** Simulated and calculated capacitance versus number of fingers.

Table 2. Calculated versus measured capacitance values

Method	Capacitance value
Calculated	299 pF
Measured	296 pF

Table 3. Calculated, simulated, and measured inductance values for both proposed spiral inductors

Method	Circular inductance	Rectangular inductance
Calculated	594 nH	26.76 μH
Simulated	437 nH	20.165 μH
Measured	550 nH	24 μH

for an outer width and length of 37.7 and 62.6 mm, respectively, two thicknesses of 0.2 and 0.4 mm, 22 turns with a gap of 0.2 mm. Taking into consideration the parameters of the Kapton substrate of a relative dielectric of 3.4 and a loss tangent of 0.0036.

Tag circuits and systems

The circuit diagram of the proposed low-cost RFID system including the reader and charger is shown in Fig. 7. In addition to accurate planar thin-film passive circuit element design methodologies described in previous sections, associated peripheral

detector and charger circuits are also discussed in detail in this section. The reader design involves a single Bluetooth Low-Energy (BLE) IC as a full controller and communication device. Simple fully differential 3 MHz signals are applied to a series network of a 200 Ω total resistor and a PCB-trace detector receive coil L_{rx} of about 20 turns. The 100 Ω insulation resistors serve two purposes. First, they limit the current to be drawn from the BLE GPIO drivers, which is not a significant amount for the low-power IC and hence allow an optimal voltage swing. Second, they form an intermediate variable impedance measurement taps for the RX detector coil to allow sensing of the variable load resulting from various planar tag inductive resonance circuits inserted. In order to enhance the effective coupling between the reader and the tag, center gap for the reader coil is aligned with the center gap of the tag which is arranged to be matching by design. In order to minimize the user read out errors, the notes are inserted into a guided sandwiched upper and lower double-plated PCB coil structure with 1.5 mm gap, which effectively eliminates the gap errors in the vertical direction. In the direction of insertion, the notes progress stops at the sidewall removing these variations, as well. The last variation, which is responsible for the largest reading error source, relates to the shifts toward the sides in the horizontal plane. In order to minimize this shift error, the center gap of the reader coil is made slightly larger to accommodate 7–10 mm shifts. Even if a larger shift were to be exerted by the user, the optical detector determines this case easily and asks the user to insert the note properly. The only thing that varies on the tag side is the number of turns as well as the capacitive load resulting in a distinct level of attenuation in the detected signal. In order to keep stable alignment with repeatable and distinguishable load detection levels; the thin film tags are expected to be inserted between two fixed-gap PCBs. The sense path

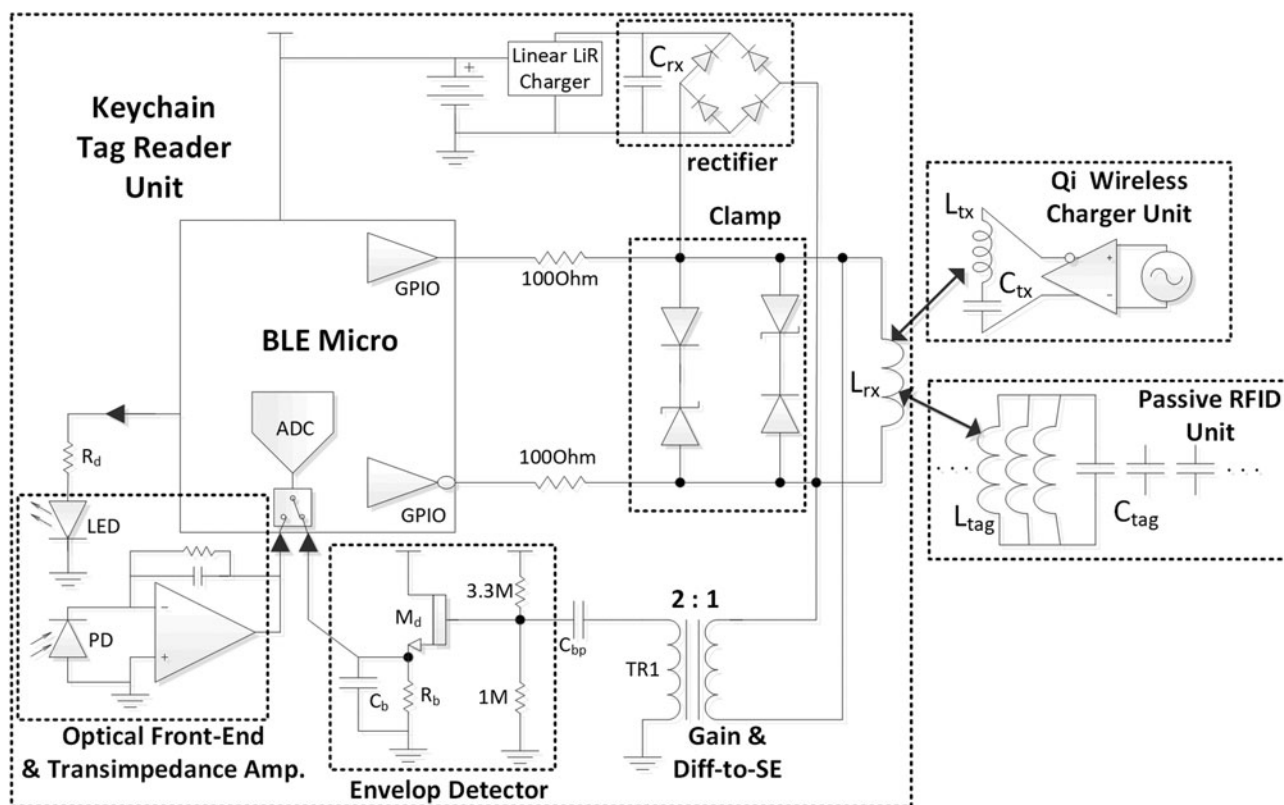


Fig. 7. RFID system circuits diagram along with the reader and the charger circuits.

to this differential coil is a differential to single-ended conversion transformer TR1 with 1:2 turn-ratio, which is chosen to both amplify the detected load difference voltage into a high impedance load of peak detector NMOS gate and also to achieve proper isolation into the DC bias levels set in the envelope peak detector. The output of this peak detector is fed into the analog to digital converter

(ADC) of the BLE for the final decision. The receiver coil is not only used to detect the unique tag RFIDs but it is also used to charge the unit wirelessly. Since the design is a fully sealed waterproof unit, the embedded 3.7 V Lithium-Polymer battery needs to be charged wirelessly. A standard Q_i charger is able to charge the unit with a 175 kHz tone, even without a secondary side resonant

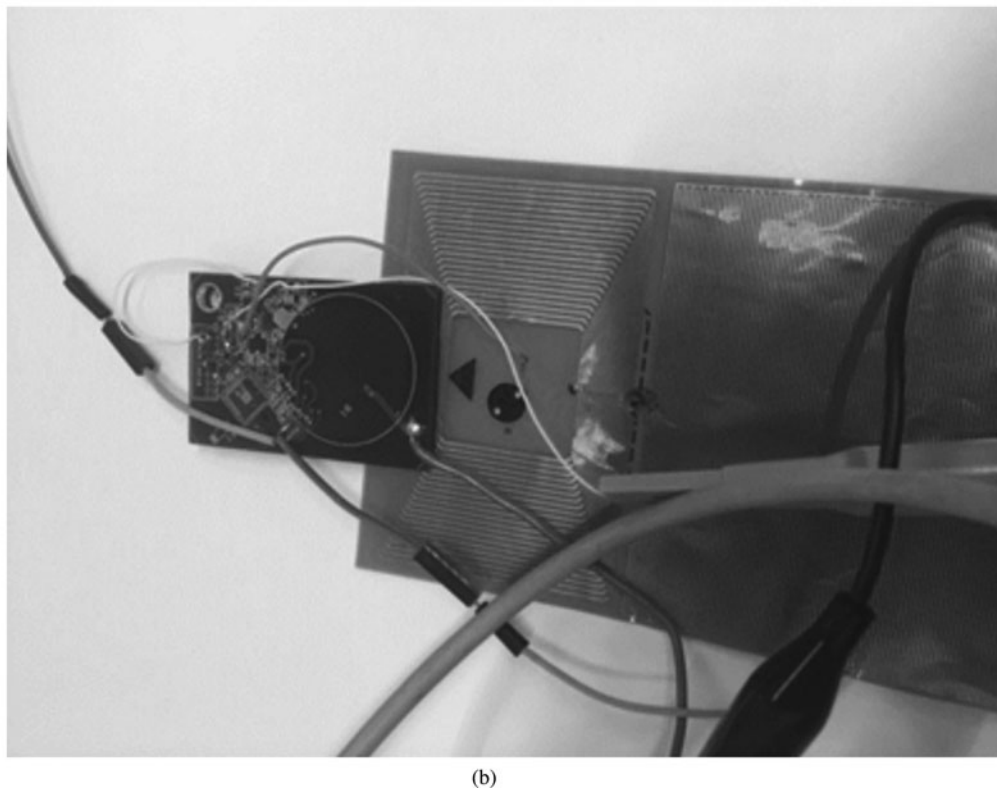
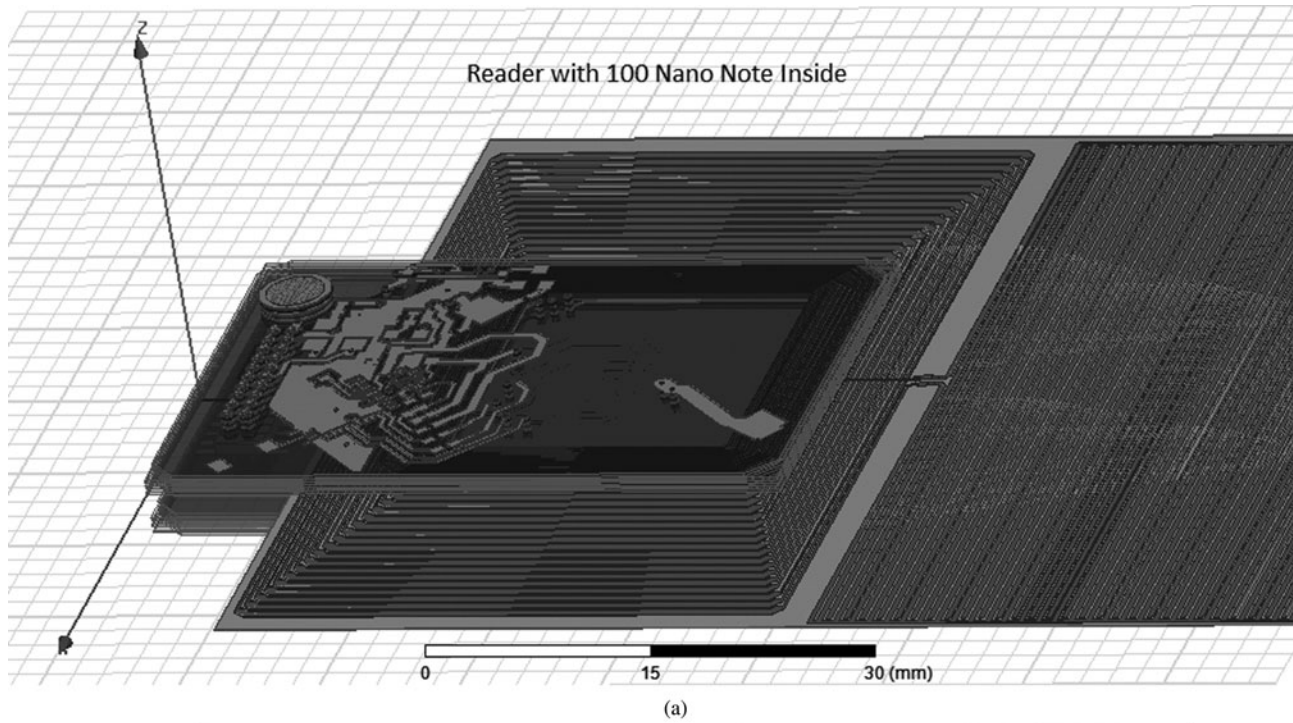


Fig. 8. The proposed system in detection mode when the tag is inserted.

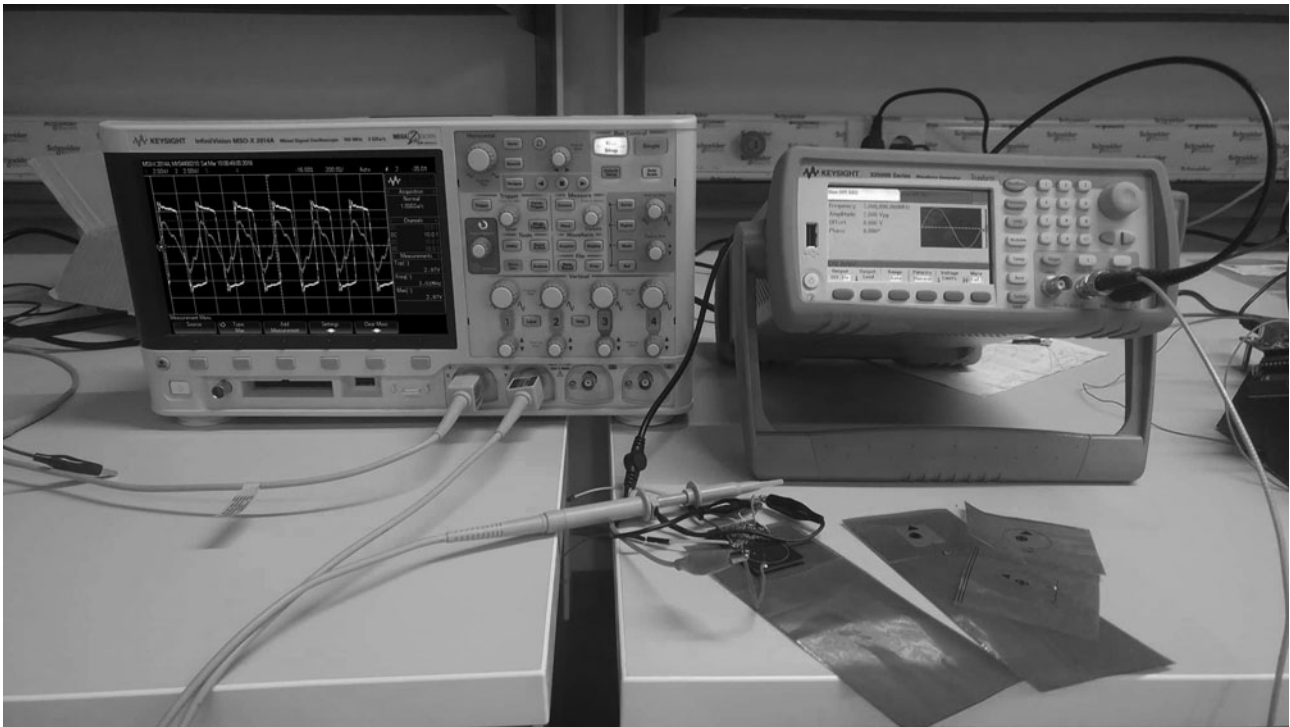


Fig. 9. Voltage difference measurements setup for tag B.

tuning capacitor. It should be noted that the coil itself had to be kept wideband without any resonance not to impact the regular sensing operation of a wide frequency range of various tag coils, while simultaneously charging the battery with a safe margin. Two-way differential Zener clamp circuitry is used to protect the BLE chip, in case a large Q_i charging field is encountered. The Zener clamp voltage level was set around 5.9 V which allows large enough headroom for the Lithium battery charger circuit after the rectifier diode drops and does not push the devices into breakdown regions if the charging field happens to be excess in strength (Fig. 8).

The last circuit in the detector system is an optical front-end which is responsible for sensing the light intensity variation that results from the various minimum size via patterns engraved in the center of the coil in the tag. On the corresponding region of the bottom PCB of the two-layer detection circuit is a no solder mask reflector metal area that reflects the light that is produced on the top PCB. A photo-diode and light-emitting diode (LED) pair combo device on the back of this top PCB is activated by the controller during the tag readout, detecting the level of light that can go through and reflect back. In the corresponding area of the Kapton film tag, there exists a hole pattern with dark black silkscreen to improve the sensitivity of this low-cost detection mechanism. A small photodiode current is amplified through a trans-impedance amplifier and fed into the ADC for the final level decision in the microcontroller.

Measurements

After elaborating on the functionality of the proposed system circuitry, this section discusses the measurement results of the proposed system. As mentioned before that the system has two identification criterions; one is measuring the change in peak voltage due to the inserted resonant tag load; the other is

measuring the equivalent current intensity due to the reflected light intensity between the reader and the tag corresponding to the hole pattern of the proposed via structure. This section will discuss the results of the two detection methods separately.

Voltage difference detection

As illustrated in Fig. 9 of the measurement setup, the reader is fed by a 3 MHz square wave of 4-Volt peak-to-peak differential signal. The screenshot demonstrates the output on the oscilloscope for the given three cases, no tag inserted, tag A case, and tag B case; two distinct prototypes that were manufactured for test purposes.

There was 500 mV of a received signal-level difference between the tags as shown in Fig. 10, where the signal level drops from 3.3 to 3 V in the case of tag A as a load and it drops to 2.5 V in the case of tag B, with a dynamic range of 500 mV without even amplification. Hence, the design provides flexibility to design eight different structures to correspond to eight different tag designs with safe margins. From this specific RF-based detection mechanism, 3-bit extraction is used to identify the uniqueness of each particular tag, with a Least Significant Bit (LSB) of 65 mV which could be easily differentiated using the ADC in the controller.

Current intensity detection measurements

This particular detection mechanism measures the photo-diode current level corresponding to the reflected light intensity resulting from the hole pattern implemented on the tags. In Fig. 11, trans-impedance amplifier output measurements corresponding to a number of holes in the patterns of tag A and tag B are illustrated by the black solid line showing a quiet linear behavior with

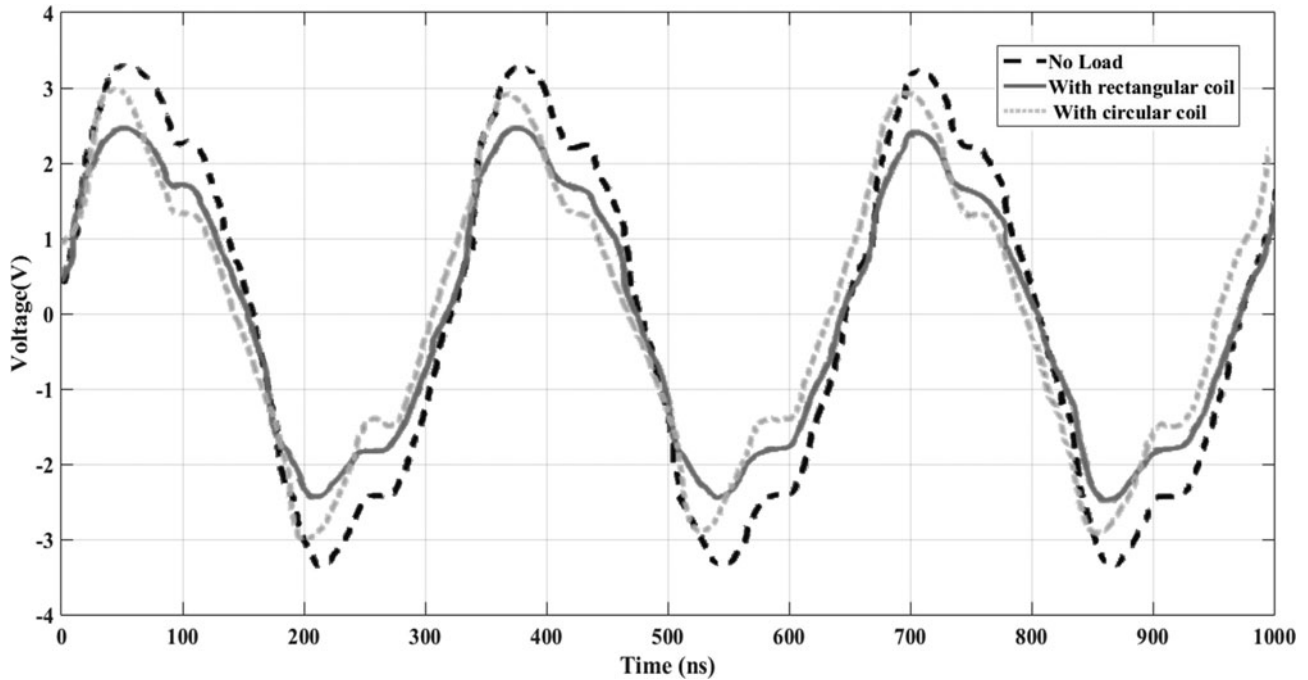


Fig. 10. Voltage levels measured after insertion of the proposed tag loads.

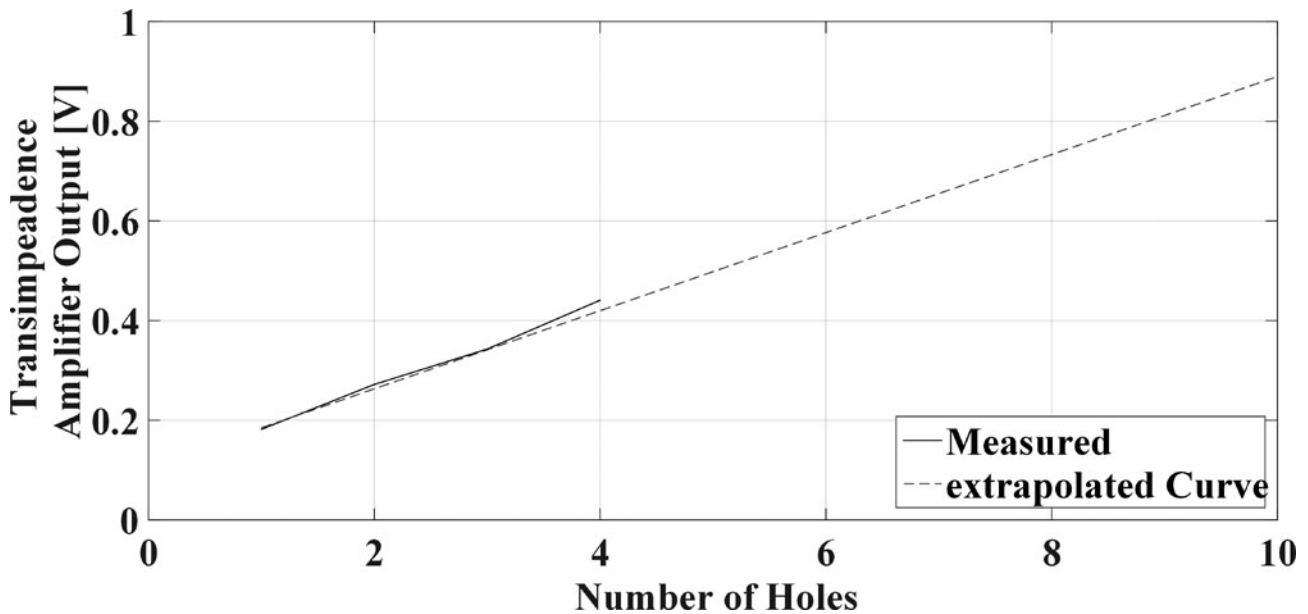


Fig. 11. Trans-impedance Amp. output versus number of holes.

Table 4. Comparison with published works

Point of Comparison	[6] SISY 2012	[20] EuCap 2014	[21] Prime Asia 2018	This work
Kind of RFID	Passive lumped	Passive dipole	Active	Passive lumped
Communication range	Remote coupled	Long (100 cm)	NFC	Close coupled
Operational frequency	125 KHz	2–5 GHz	13.56 MHz	3 MHz
Substrate	Flexible Kapton	TF290 non-flexible	Flexible PET	Flexible Kapton
Cost	Low	Moderate	High	Low
Number of layers	2 layers	1 layer	1 layer	1 layer

the dashed interpolation line. It is possible to extrapolate these initial test results with a limited number of holes from the mentioned two test tags to conclude with up to 32 holes for safe detection dynamic range. This provides an additional 5-bit variety in a number of distinct tags that can be constructed.

Conclusion

This paper described a low-cost and robust low-power RFID tag and a reader technology for many daily activities such as tickets, gaming, temporary activity tags, etc. The tags could be produced in a standard single-layer copper-clad flexible substrate production technology without any component or assembly requirement. The tags are just planar printed circuits and hole patterns, while the wireless charging reader is designed as simple as two sandwich layers of two-layer each FR-4 PCBs housing all the reading circuits and PCB trace coils. A water-proof and stress-proof feature of the proposed design allows it to be used in the form of a keychain that can be carried along everywhere by individual users. Table 4 illustrates the differences between the proposed work and other published works.

Acknowledgements. The authors would like to thank Mert Karaca of Microelectronics Labs at Özyeğin University for his help in accurate impedance measurement and characterizations of the designed TAG units.

References

- Finkenzeller K (2010) *RFID Handbook: Fundamentals and Applications in Contactless Smart Cards, Radio Frequency Identification and Near-Field Communication*. UK: John Wiley & Sons.
- Karmakar NC, Roy SM, Preradovic S, Vo TD and Jenvey S (2006) Development of low-cost active RFID tag at 2.4 GHz. *Microwave Conference, 2006. 36th European*, IEEE, pp. 1602–1605.
- Silva PM, Sousa FR and Plett C (2018) On-Chip Automatic LC Tuner for RFID Tags Based on Negative Resistances. *IEEE Transactions on Circuits and Systems II: Express Briefs* 65, 1029–1033.
- Preradovic S, Karmakar NC and Balbin I (2008) RFID transponders. *IEEE Microwave Magazine* 9, 90–103.
- Kisic M, Dakic B, Damnjanovic M, Menicanin A, Blaz N and Zivanov L (2013) Design and simulation of 13.56 MHz RFID tag in ink-jet printing technology. pp. 263–267, 05.
- Dakic B, Damnjanovic M, Zivanov L, Menicanin A, Blaz N and Kisic M (2012) Design of RFID antenna in ink-jet printing technology. *Intelligent Systems and Informatics (SISY), 2012 IEEE 10th Jubilee International Symposium on*, IEEE, pp. 429–432.
- Herrojo C, Mata-Contreras J, Paredes F and Martin F (2017) Near-field chipless RFID encoders with sequential bit reading and high data capacity. *Microwave Symposium (IMS), 2017 IEEE MTT-S International*, IEEE, pp. 1564–1567.
- Benamara M, Grzeskowiak M, Diet A, Conessa C, Lissorgues G and Le Bihan Y (2018) Effect of added resonators in RFID system at 13.56 MHz. *IET Microwaves, Antennas & Propagation* 12, 684–691.
- Preradovic S and Karmakar NC (2010) Design of chipless RFID tag for operation on flexible laminates. *IEEE Antennas and Wireless Propagation Letters* 9, 207–210.
- Mukherjee S (2007) Chipless radio frequency identification by remote measurement of complex impedance. *Microwave Conference, 2007. European*, IEEE, pp. 1007–1010.
- Hota M, Bera M and Maiti C (2012) Flexible metal–insulator–metal capacitors on polyethylene terephthalate plastic substrates. *Semiconductor Science and Technology* 27, 105001.
- Meena JS, Chu M-C, Kuo S-W, Chang F-C and Ko F-H (2010) Improved reliability from a plasma-assisted metal–insulator–metal capacitor comprising a high-k hfo₂ film on a flexible polyimide substrate. *Physical Chemistry Chemical Physics* 12, 2582–2589.
- Blaž N, Kisić M, Žlebić Č, Marić A and Živanov L (2016) Capacitance variation of inkjet printed interdigital capacitor by structure bending. *Electronics Technology (ISSE), 2016 39th International Spring Seminar on*, IEEE, pp. 506–509.
- Huang G-L, Sim C-Y-D, Liang S-Y, Liao W-S and Yuan T (2018) Low-profile flexible UHF RFID Tag design for wristbands applications. *Wireless Communications and Mobile Computing* 2018, Article ID 9482919, 13 pages.
- Jang H, Lim W, Oh K, Moon S and Yu J (2010) Design of low-cost chipless system using printable chipless tag with electromagnetic code. *IEEE Microwave and Wireless Components Letters* 20, 640–642.
- Sheeparamatti BG, Hanasi PD, Aibbigeri V and Meti N (2015) Study of capacitance in electrostatic comb-drive actuators. In *Excerpt from the Proceedings of the COMSOL Conference in Pune*.
- Igreja R and Dias C (2004) Analytical evaluation of the interdigital electrodes capacitance for a multi-layered structure. *Sensors and Actuators A: Physical* 112(2–3), 291–301.
- Khan AM and Reddy M (2016) Design and optimization of interdigital capacitor. *International Journal of Research in Engineering and Technology* 5, 73–78.
- Mohan SS, del Mar Hershenson M, Boyd SP and Lee TH (1999) Simple accurate expressions for planar spiral inductances. *IEEE Journal of Solid-State Circuits* 34, 1419–1424.
- Nair R, Barahona M, Betancourt D, Schmidt G, Bellmann M, Höft D, Plettmeier D, Hübler A and Ellinger F (2014) A fully printed passive chipless RFID tag for low-cost mass production. *The 8th European Conference on Antennas and Propagation (EuCAP 2014)*, The Hague.
- Yuan M, Ghannam R, Karadimas P and Heidari H (2018) Flexible RFID Patch for Food Spoilage Monitoring. In *2018 IEEE Asia Pacific Conference on Postgraduate Research in Microelectronics and Electronics (PrimeAsia)*, pp. 68–71. IEEE.



Salma El-Sawy was born in Egypt, received her B.Sc. degree from Ainshams University (Egypt) Faculty of Engineering, Electronics and Communication Department in 2013. In 2014, she joined CST Middle east as a verification and research engineer. She moved to Istanbul and joined Özyeğin University electric and electronic department in 2017 to pursue her M.Sc. degree. Her main interests include circuit designs, analog, and mixed signals integrated circuits design.



Wasim Nawaz received his undergraduate degree in Electrical Engineering from Pakistan's high ranking engineering institute, Pakistan Institute of Engineering and Applied Sciences (PIEAS) in 2013. After that, he worked in a research organization for more than 3 years. His main area of research is RF front end including antennas and passive microwave circuits. Except for this research, his work is already presented and published in IEEE International conferences including ICASE (2015), ICS (2016), and ComTECH (2017). Apart from R&D in the field of Antennas and Microwave, he also has in-depth knowledge and experience on testing antenna systems in anechoic chamber and near-field scanning facility. Currently he is a graduate student of the Department of Electrical and Electronics Engineering at Özyeğin University and working as an RF Front End Engineer at Analog and RF Labs under the supervision of Dr. Ahmet Tekin.



Mohamed Osama was born in Cairo, Egypt in 1992. He received the B.Sc. degree in Electrical and Communication Engineering from Cairo University, in 2014. In 2016, he started his M.Sc. degree at Ozyegin University. In 2014, he received the second best graduation project prize sponsored by Mentor Graphics in Egypt. In 2016, he received full scholarship including housing from Ozyegin University where he is currently pursuing his M.Sc. degree. From 2014 to present, he is working as a firmware developer at WaveWorks Inc. His research interests include RF, analog circuit design, power amplifiers, and biomedical electronic devices.



Ahmet Tekin has received his EE Ph.D. degree from the University of California Santa Cruz, CA, USA; EE MS degree from North Carolina A&T State University, Greensboro, NC, USA; and EE BS degree from Bogazici University, Istanbul, Turkey in 2008, 2004, and 2002, respectively. In addition to academic research in microelectronics, he worked for multiple innovative semiconductor design companies such as Multigig, Inc., Newport Media, Aydeekay LLC, Broadcom corp., Semtech Corp., Nuvoton Technology Corp., Qualcomm and Waveworks Inc., leading designs for communications, consumer, and medical markets. His main focus area is analog/RF/mixed-signal integrated circuit design for communication and biomedical applications. He is currently the head of Analog&RF Labs at Özyeğin University and serves in the board of directors of Waveworks Inc., Mission Viejo, CA, USA.